Dalton Transactions

ROYAL SOCIETY OF CHEMISTRY

PAPER

View Article Online
View Journal | View Issue

Check for updates

Cite this: *Dalton Trans.*, 2023, **52**, 17942

Filling the gaps of uranium oxide hydrates with magnesium(II) ions: unique layered structures and the role of additional sodium(I) ions†

Yingjie Zhang, *[a] Kimbal T. Lu,[a,b] Tao Wei,[a] I. Karatchevtseva[a] and Rongkun Zheng [b]

Received 20th September 2023,
Accepted 9th November 2023

DOI: 10.1039/d3dt03078d

rsc.li/dalton

Alkaline earth metal ions play an important role in the formation of secondary uranium minerals due to their abundance in the Earth's crust. Although uranium oxide hydrate (UOH) minerals and synthetic phases with calcium, strontium and barium ions have been investigated, their counterparts with magnesium ions are much less studied. In this work, synthetic UOH materials with magnesium ions have been investigated with three new compounds being synthesised and characterised. Compound $Mg_2(H_3O)_2(H_2O)_6[(UO_2)_3O_4(OH)]_2$ (**U-Mg1** with a U : Mg ratio of 3 : 1) crystallises in the monoclinic $P2_1/c$ space group having a layered crystal structure, constructed by β-U_3O_8 layers with 6-fold coordinated Mg^{2+} ions as interlayer cations. Compound $Na_2Mg(H_2O)_4[(UO_2)_3O_3(OH)_2]_2$ (**U-Mg2p** with U : Mg : Na ratios of 6 : 1 : 2) crystallises in the triclinic $P\bar{1}$ space group having a layered structure, constructed by a unique type of uranium oxide hydroxide layer containing both α-U_3O_8 and β-U_3O_8 features, with alternating layers of 6-fold coordinated Mg^{2+} and 6-/8-fold coordinated Na^+ interlayer cations. Compound $Na_2Mg(H_2O)_4[(UO_2)_4O_3(OH)_4]_2$ (**U-Mg2n** with U : Mg : Na ratios of 8 : 1 : 2) crystallises in the triclinic $P\bar{1}$ space group having a corrugated layer structure, constructed by a unique type of uranium oxide hydroxide layer with mixed 6-fold coordinated Mg^{2+} and 7-fold coordinated Na^+ interlayer cations. The structural diversity in the UOH-Mg system was achieved by adjusting the solution pH using NaOH, highlighting the importance of solution pH control and the additional Na^+ ions in the formation of UOH phases. The extra structural flexibility offered by the Na^+ ions emphasizes the opportunity for synthesising UOHs with dual-cations to further improve our understanding of the alteration products of spent nuclear fuel under geological disposal.

1. Introduction

Nuclear energy has resumed a growing momentum worldwide owing to the increasing demand for cleaner energy.[1] However, the major technical challenge for the nuclear energy sector is the safe treatment and disposal of spent nuclear fuel (SNF).[2,3] The most acceptable approach is the direct geological disposal of the SNF in a stable underground repository.[4–6] Although UO_2 as the primary component of SNF is stable under the reducing environment in an underground repository, it can undergo severe alterations (oxidation and hydration) if exposed to air.[7,8]

It is well understood that uraninite (UO_{2+x}) as a primary uranium mineral or UO_2 as the primary component of SNF will be gradually oxidised from U^{4+} to U^{6+} if exposed to oxidative conditions.[9–11] As the most stable U^{6+} form, the uranyl [$(UO_2)^{2+}$] ion with two strongly bonded axial oxygen atoms is ready to coordinate with O/OH ligands in the equatorial positions forming tetragonal, pentagonal and hexagonal bipyramids, which connect each other *via* both corner- and edge-sharing to form various uranyl-containing compounds, normally in the form of layered structures with various interlayer cations adopted from the surroundings.[12–15]

Uranium oxide hydrate (UOH) minerals are a group of secondary uranium minerals formed in the early stage of uraninite weathering.[3,14–16] They provide a direct natural analogue to the SNF alterations under geological disposal. The recent campaign for a better understanding of UOH materials has led to the discovery of dozens of UOH minerals[14–16] and about two

[a]*Australian Nuclear Science and Technology Organisation, Locked Bag 2001, Kirrawee DC, NSW 2232, Australia. E-mail: yzx@ansto.gov.au*
[b]*School of Physics and Advanced Materials, University of Sydney, Ultimo, New South Wales 2007, Australia*

†Electronic supplementary information (ESI) available: SEM-EDS and supporting tables. CCDC 2289968 (**U-Mg1**), 2289969 (**U-Mg2p**), and 2289970 (**U-Mg2n**). For ESI and crystallographic data in CIF or other electronic format see DOI: https://doi.org/10.1039/d3dt03078d

dozen synthetic UOH compounds.[14–16] Most of these UOH materials have layered structures containing uranium oxide hydroxide layers with interlayer cations. As such, they differ mainly in two aspects: the O/OH ratio in the uranium oxide hydroxide layers and the type of interlayer cation. For UOH minerals, the secondary cations are mainly alkali,[17,18] alkaline earth and p-block cations such as Pb due to their natural abundance or are located at the end of the U decay chain.[19–22] In addition, the uranyl oxide hydroxide layer topologies for various UOH minerals have been comprehensively reviewed.[23] In addition, synthetic UOH materials with a wide range of secondary cations including alkali,[24,25] alkaline earth,[26–29] lead,[30] transition metals[31–33] and lanthanide ions[34–36] have been reported. Furthermore, synthetic UOH phases with interlayer anions are also possible, although less studied.[37]

Apart from the dominant layered UOH structures, several types of complicated three-dimensional (3D) structures have also been discovered.[30,38,39] Among them is a framework-type structure with uranyl species acting as bridging ligands between the uranium oxide hydroxide layers to form uranium oxide hydrate frameworks (UOHFs).[40] The main feature of UOHFs is their structural flexibility as the large framework channels are capable of incorporating a range of secondary cations from 1+ to 4+ including $(NH_4)^+$, Pb^{2+}, Sr^{2+}, Y^{3+}, Er^{3+}, Sm^{3+}, Eu^{3+}, Gd^{3+} and U^{4+}.[39–43] The complexity arising from UOHFs highlights the need to study these materials further to better comprehend the uranium hydrolysis chemistry in the presence of various secondary cations.

Magnesium (Mg), as the eighth most abundant element in the Earth's crust (~2%), exists in more than 60 minerals.[44] Consequently, it is the third most plentiful element dissolved in seawater.[44] Unlike the other larger alkaline earth cations (Ca^{2+}/Sr^{2+}/Ba^{2+}), the relatively smaller ionic radius of Mg^{2+} makes it behave quite differently. In fact, it adopts 6-fold coordination in an octahedral geometry similar to bivalent transition metal ions.[45] Despite the fact that the Mg^{2+} ion has been found in more than 30 uranyl minerals[46] such as silicates, sulphates, phosphates *etc*., and also in the UOH mineral richetite,[47] its exact role in the formation of UOH minerals and synthetic phases has not been well established. Earlier works were focused on the synthesis of UOH-Mg by hydrothermal reactions of schoepite with magnesium nitrate/sulphate, leading to the formation of two types of UOHs with Mg^{2+} ions, one with U : Mg = 6 : 1 [48] and the other with U : Mg = 3 : 1.[49] However, the detailed crystal structures remain unknown. In addition, some UOH minerals have been found to contain M^{2+} (M = Ca, Sr, Ba, Pb) ions together with Na^+ ions,[50,51] and the role of the additional Na^+ ions in the formation and stabilisation of such UOH structures requires further research.

In this work, we report the synthesis and characterisation of three novel UOH compounds containing Mg^{2+} ions with/without Na^+ ions. They have three different types of layered structures revealed by synchrotron single crystal X-ray diffraction. The diversity of uranium oxide hydroxide layers has been achieved at nearly neutral solution pH values adjusted with a diluted NaOH solution, highlighting the importance of controlling the solution pH and the additional Na^+ ions in the formation and stabilisation of UOH phases with Mg^{2+} ions. Subsequently, their microstructures and spectroscopic properties have been investigated using scanning and transmission electron microscopy, Raman spectroscopy and diffuse reflectance spectroscopy.

2. Experimental

2.1. Syntheses of materials

Uranyl nitrate hexahydrate with uranium in natural isotopic abundance was used. Materials containing uranium are radioactive and should be handled with care in regulated facilities. Other chemicals of A.R. grade were purchased from Sigma-Aldrich (Merck).

2.1.1 $Mg_2(H_3O)_2(H_2O)_6[(UO_2)_3O_4(OH)]_2$ (U-Mg1). Uranyl nitrate hexahydrate (0.0503 g, 0.1 mmol) and magnesium nitrate hexahydrate (0.0516 g, 0.2 mmol) were dissolved in 5 mL of deionised water (DIW), followed by adjusting the solution pH to 7.50 with a dilute NaOH solution. The mixture was then transferred into a 30 mL Teflon vessel, sealed in a steel autoclave and heated in an oven at 200 °C for 24 h. The orange crystalline compound **U-Mg1** was obtained after cooling (10 °C h^{-1}) to ambient temperature with the final solution pH of 6.52, washed with DIW and dried in air at ambient temperature with ~76 wt% yield (0.025 g).

2.1.2 $Na_2Mg(H_2O)_4[(UO_2)_3O_3(OH)_2]_2$ (U-Mg2p) and $Na_2Mg(H_2O)_4[(UO_2)_4O_3(OH)_4]_2$ (U-Mg2n). Similar to the synthesis of **U-Mg1**, 0.1 mmol of uranyl nitrate hexahydrate and 0.2 mmol of magnesium nitrate hexahydrate were dissolved in 5 mL of DIW, followed by adjustment of the solution pH to 8.08 with a dilute NaOH solution. The mixture was then transferred into a 30 mL Teflon vessel, sealed in a steel autoclave and heated in an oven at 200 °C for 24 h. Compounds **U-Mg2p** (plate crystals) and **U-Mg2n** (needle crystals) were obtained in one pot after cooling (10 °C h^{-1}) to ambient temperature with the final solution pH of 8.06, and separated manually from the reaction mixture for single crystal X-ray diffraction and limited microanalyses.

2.2. Characterisation

2.2.1 Synchrotron single crystal X-ray diffraction. The single crystal data for compounds **U-Mg1** (CCDC 2289968), **U-Mg2p** (CCDC 2289969) and **U-Mg2n** (CCDC 2289970)† were collected at 100(2) K on the MX2 beamline[52] at the Australian Synchrotron employing silicon double crystal monochromated synchrotron radiation (λ = 0.71089 Å). Data integration and reduction were undertaken with XDS.[53] Absorption corrections were applied to the data using SADABS.[54] The structures were solved by direct methods[55] and refined with SHELXL-2014 [56] using the Olex^2 graphical user interface.[57] All but hydrogen atoms were located on the electron density map and refined anisotropically. The one-circle goniometer on the MX2 beamline offered less redundant data for effective absorption corrections. As such, some strong Q-peaks exist around U atoms,

which is quite common for uranium oxide materials. The residual peaks could be due to unmodeled disorder or twinning. Such artifacts have consequences including systematic errors in bond distances (which affect BVS analysis) and possible element misidentification in some cases.

2.2.2 Scanning electron microscopy (SEM) and transmission electron microscopy (TEM). The crystal morphologies and elemental compositions were analysed using SEM coupled with energy dispersive spectrometry (EDS). Samples were carbon coated and examined in a Zeiss Ultra Plus SEM (Carl Zeiss NTS GmbH, Oberkochen, Germany) operating at 15 kV equipped with an Oxford Instruments X-Max 80 mm^2 SDD X-ray microanalysis system. Small amounts of finely ground crystal fragments were suspended in ethanol and then dispersed on a TEM holey-carbon film with copper support. The specimens were characterized using a JEOL 2200FS (JEOL Ltd, Japan) TEM operated at 200 kV, fitted with an Oxford X-Max silicon drift detector for energy dispersive X-ray analysis.

2.2.3 Raman spectroscopy. Raman spectra were collected on a Renishaw inVia spectrometer equipped with a 785 nm Ar laser in the range of 1000–100 cm^{-1} with a spectral resolution of ~1.7 cm^{-1}.

2.2.4 Diffuse reflectance spectroscopy (DRS). The absorption spectra in the UV-visible region were recorded on an Agilent Cary 5000 spectrophotometer equipped with a Labsphere Biconical Accessory and referenced to a Labsphere certified standard.

3. Results and discussion

3.1. Material synthesis and characterisation

All compounds were synthesised hydrothermally at 200 °C for 24 h with uranyl and magnesium nitrates, and the solution pH was adjusted to above neutral using a dilute NaOH solution. When the initial solution pH values were below 7.0, only metaschoepite was identified based on the SEM-EDS analysis. **U-Mg1** was formed with the final solution pH of 6.52 while **U-Mg2p** and **U-Mg2n** were formed in one pot with the final solution pH of 8.06. Both syntheses were repeated with good reproducibility. The synthesis conditions and final products are summarised in Table 1.

SEM-EDS examination of **U-Mg1** confirmed the thin plate crystal morphology (Fig. 1a) and the presence of U, Mg and O, with a U : Mg atomic ratio of 3 : 1 (Fig. S1, ESI†). Similarly, SEM-EDS analysis of **U-Mg2p** (plate crystals in Fig. 1b) and **U-Mg2n** (needle crystals in Fig. 1b) confirmed the presence of U, Mg, Na and O with U : Mg : Na atomic ratios of 6 : 1 : 2 for **U-Mg2p** (Fig. S2, ESI†) and 8 : 1 : 2 for **U-Mg2n** (Fig. S3, ESI†), respectively.

Table 1 Synthesis conditions for compounds **U-Mg1**, **U-Mg2p** and **U-Mg2n**

			Synthesis conditions		Final product		
Compound	Precursors	U : Mg	Initial pH	Temp. Time	Formula	pH	U : Mg : Na O : OH
U-Mg1	$UO_2(NO_3)_2{\cdot}6H_2O$	1 : 2	7.50	200 °C, 24 h	$Mg_2(H_2O)_8[(UO_2)_3O_2(OH)_3]_2$	6.52	3 : 1 : 0 4 : 1
U-Mg2p	$Mg(NO_3)_2{\cdot}6H_2O$		8.08		$Na_2Mg(H_2O)_4[(UO_2)_3O_3(OH)_2]_2$	8.06	6 : 1 : 2 3 : 2
U-Mg2n	NaOH		8.08		$Na_2Mg(H_2O)_4[(UO_2)_4O_3(OH)_4]_2$	8.06	8 : 1 : 2 3 : 4

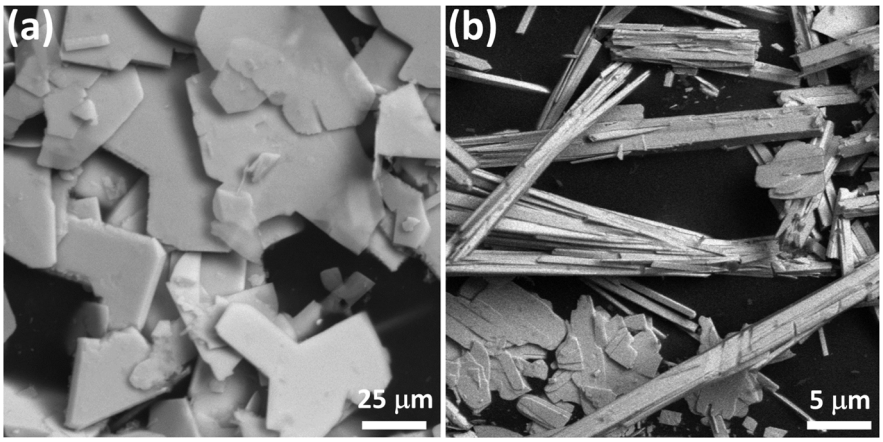

Fig. 1 Backscattered SEM images of **U-Mg1** (a), **U-Mg2p** (plate crystals) and **U-Mg2n** (needle crystals) (b).

3.2. Crystal structures and discussion

The crystal data and structure refinement details for **U-Mg1**, **U-Mg2p** and **U-Mg2n** are summarised in Table 2, with selected bond lengths (Å) and angles (°) listed in Tables 3–5, respectively. **U-Mg1** crystallises in the monoclinic $P2_1/c$ space group. It has a layered crystal structure (Fig. 2) constructed with β-U_3O_8 type uranium oxide hydroxide layers (Fig. 2b) and interlayer Mg^{2+} species (Fig. 2a). There are six distinct U centres, two in 6-fold coordination (U1 and U4) and four in 7-coordination (U2, U3, U5 and U6), and two Mg centres both in 6-fold coordination. Although U1 and U4 are in 6-fold coordination, they differ remarkably. U1 lacks uranyl nature with six U–O bonds ranging from 2.055(18) to 2.136(18) Å while U4 has two shorter U═O distances from 1.887(19) to 1.960(19) Å with an O═U═O angle of 178.7(7)° and four longer U–O distances in the equatorial plane ranging from 2.154(18) to 2.192(18) Å, suggesting the presence of a uranyl unit with elongated U═O bonds. All U2, U3, U5 and U6 are typical uranyl centres in a pentagonal bipyramidal geometry, with U═O bond lengths for the uranyl moieties ranging from 1.797(18) to 1.835(18) Å and O═U═O angles from 174.9(8)° to 178.3(8)°. The U–O distances in the equatorial planes range from 2.252(18) to 2.383(18) Å. The two Mg centres are separated without any direct interaction, both 6-fold coordinated in an octahedral geometry with Mg–O distances ranging from 2.00(2) to 2.09(2) Å. These U–O and Mg–O bonds are consistent with literature data.[45] The distance between layers is ~4.05 Å measured *via* the two apical oxygen atoms of the Mg octahedra.

While the bending of the uranyl unit for U5 [174.9(8)°] is obvious, the phenomenon is often observed in uranyl-containing compounds.[15] The coordination environment for U1 is unusual in that it does not involve a uranyl species. In fact, it has a tetraoxido core coordination environment and can be either U(v) or U(vi) depending on the six U–O bond lengths.[58,59] However, similar U centres have been found in

Table 2 Crystal data and structure refinements for **U-Mg1**, **U-Mg2p** and **U-Mg2n**

Compound	**U-Mg1**	**U-Mg2p**	**U-Mg2n**
CCDC	2289968	2289969	2289970
Empirical formula	$Mg_2O_{30}U_6$	$MgNa_2O_{26}U_6$	$MgNa_2O_{34}U_8$
Formula weight	1956.80	1914.47	2518.53
Crystal system	Monoclinic	Triclinic	Triclinic
Space group	$P2_1/c$	$P\bar{1}$	$P\bar{1}$
a (Å)	8.6310(17)	7.0150(14)	8.2140(16)
b (Å)	28.231(6)	12.067(2)	8.3980(17)
c (Å)	10.601(2)	13.411(3)	10.769(2)
α/(°)	90	91.22(3)	77.62(3)
β/(°)	105.99(3)	100.49(3)	89.01(3)
γ/(°)	90	90.36(3)	75.83(3)
Volume (Å^3)	2483.1(9)	1116.0(4)	703.0(3)
Z/μ (mm^{-1})	4/39.162	2/43.558	1/46.071
Min./max. θ [°]	1.443/24.997	1.545/24.995	1.935/24.995
d_{calcd} (g cm^{-3})	5.234	5.697	5.949
GOF	1.125	1.076	1.019
Final R_1 [a] [$I > 2\sigma(I)$]	0.0645	0.0401	0.0424
Final wR_2 [b] [$I > 2\sigma(I)$]	0.1583	0.1023	0.1058

[a] $R_1 = \sum||F_o| - |F_c||/|F_o|$. [b] $wR_2 = \{\sum[w(F_o^2 - F_c^2)^2]/\sum[w(F_o^2)^2]\}^{1/2}$.

Table 3 Selected bond lengths and angles for compound **U-Mg1**

Bond	Length (Å)	Bond	Length (Å)	Bond	Length (Å)
U1–O1	2.055(18)	U2–O8	1.816(18)	U3–O9	1.815(18)
U1–O4	2.057(18)	U2–O7	1.835(18)	U3–O10	1.841(18)
U1–O3	2.087(18)	U2–O11	2.261(18)	U3–O12[d]	2.264(18)
U1–O2	2.090(18)	U2–O6	2.287(18)	U3–O12	2.305(18)
U1–O5	2.105(18)	U2–O20[c]	2.330(18)	U3–O11	2.317(18)
U1–O6	2.136(18)	U2–O3[b]	2.341(18)	U3–O5[b]	2.334(18)
		U2–O5[b]	2.365(18)	U3–O19[e]	2.335(18)
		O7═U2═O8	178.2(8)	O9═U2═O10	177.3(8)
U4–O14	1.887(19)	U5–O17	1.797(18)	U6–O22	1.805(18)
U4–O13	1.960(19)	U5–O18	1.829(19)	U6–O21	1.840(18)
U4–O15	2.154(18)	U5–O15[f]	2.282(18)	U6–O16[e]	2.252(18)
U4–O11	2.165(18)	U5–O19	2.328(18)	U6–O20	2.311(18)
U4–O16	2.169(18)	U5–O15[g]	2.337(17)	U6–O3[e]	2.353(18)
U4–O12	2.192(18)	U5–O16[g]	2.342(18)	U6–O4[h]	2.363(18)
O13═U2═O14	178.7(7)	U5–O4[a]	2.383(18)	U6–O6[h]	2.365(18)
		O17═U2═O18	174.9(8)	O21═U2═O22	178.3(8)
Mg1–O23	2.028(19)	Mg1–O26	2.064(19)	Mg2–O28	2.036(19)
Mg1–O25	2.033(19)	Mg1–O24	2.075(19)	Mg2–O30	2.049(19)
Mg1–O9	2.05(2)	Mg2–O21	2.00(2)	Mg2–O29	2.08(2)
Mg1–O18	2.05(2)	Mg2–O8	2.03(2)	Mg2–O27	2.09(2)

[a] $1/2 + X, 3/2 - Y, -1/2 + Z$. [b] $-1/2 + X, 3/2 - Y, -1/2 + Z$. [c] $1 + X, +Y, +Z$. [d] $1 - X, 1 - Y, 1 - Z$. [e] $-1 + X, +Y, +Z$. [f] $2 - X, 1 - Y, 1 - Z$. [g] $+X, +Y, -1 + Z$. [h] $-1/2 + X, 3/2 - Y, 1/2 + Z$.

Table 4 Selected bond lengths and angles for compound **U-Mg2p**

Bond	Length (Å)	Bond	Length (Å)	Bond	Length (Å)
U1–O1	1.840(10)	U2–O7	1.819(9)	U3–O19	1.808(9)
U1–O2	1.847(9)	U2–O6	1.851(9)	U3–O18	1.813(10)
U1–O4	2.228(9)	U2–O5	2.226(8)	U3–O10	2.234(9)
U1–O3	2.235(8)	U2–O10	2.226(9)	U3–O5^{e}	2.238(9)
U1–O5	2.244(8)	U2–O4^{e}	2.266(8)	U3–O4^{e}	2.379(8)
U1–O22^{c}	2.260(9)	U2–O8	2.333(9)	U3–O9^{e}	2.386(9)
O1═U1═O2	177.8(4)	U2–O9	2.743(11)	U3–O14	2.470(9)
		O6═U2═O7	178.1(4)	O18═U3═O19	175.7(4)
U4–O12	1.828(11)	U5–O16	1.819(9)	U6–O21	1.839(10)
U4–O11	1.839(11)	U5–O15	1.822(10)	U6–O20	1.842(9)
U4–O13	2.192(9)	U5–O13	2.203(9)	U6–O13^{f}	2.231(9)
U4–O10	2.205(10)	U5–O22^{g}	2.262(8)	U6–O22	2.234(9)
U4–O9	2.363(9)	U5–O17	2.407(9)	U6–O3^{j}	2.246(8)
U4–O17^{a}	2.380(9)	U5–O3^{i}	2.436(9)	U6–O8^{c}	2.337(8)
U4–O14	2.692(9)	U5–O14	2.455(8)	U6–O17^{g}	2.683(9)
O11═U4═O12	175.2(5)	O15═U5═O16	176.9(4)	O20═U6═O21	176.2(4)
Mg1–O19	2.029(10)	Na1–O18	2.345(11)	Na2–O15^{h}	2.429(10)
Mg1–O20	2.034(10)	Na1–O6^{d}	2.384(10)	Na2–O1^{c}	2.441(11)
Mg1–O24	2.047(10)	Na1–O1^{e}	2.414(11)	Na2–O11^{d}	2.474(10)
Mg1–O25	2.069(11)	Na1–O21^{k}	2.452(10)	Na2–O11	2.590(11)
Mg1–O26	2.079(11)	Na1–O1^{b}	2.600(11)	Na2–O6	2.596(10)
Mg1–O23	2.127(10)	Na1–O6^{e}	2.672(11)	Na2–O22^{l}	2.670(12)
		Na2–O18	2.391(11)	Na2–O10	2.746(12)

^{a} 1 + *X*, +*Y*, +*Z*. ^{b} 2 − *X*, 1 − *Y*, 2 − *Z*. ^{c} 1 − *X*, 1 − *Y*, 1 − *Z*. ^{d} 1 − *X*, 1 − *Y*, 2 − *Z*. ^{e} −1 + *X*, +*Y*, +*Z*. ^{f} 1 − *X*, −*Y*, 1 − *Z*. ^{g} −*X*, −*Y*, 1 − *Z*. ^{h} 1 − *X*, −*Y*, 2 − *Z*. ^{i} −1 + *X*, −1 + *Y*, +*Z*. ^{j} 2 − *X*, 1 − *Y*, 1 − *Z*. ^{k} +*X*, +*Y*, 1 + *Z*. ^{l} 1 + *X*, +*Y*, 1 + *Z*.

Table 5 Selected bond lengths and angles for compound **U-Mg2n**

Bond	Length (Å)	Bond	Length (Å)	Bond	Length (Å)	Bond	Length (Å)
U1–O2	1.792(13)	U2–O8	1.800(12)	U3–O11	1.819(12)	U4–O14	1.813(13)
U1–O1	1.805(12)	U2–O7	1.817(11)	U3–O10	1.820(13)	U4–O13	1.861(13)
U1–O5	2.168(13)	U2–O5^{a}	2.243(13)	U3–O12	2.247(12)	U4–O15	2.207(13)
U1–O4	2.317(13)	U2–O5	2.263(12)	U3–O12^{e}	2.281(12)	U4–O12	2.169(11)
U1–O3	2.381(12)	U2–O9	2.314(13)	U3–O15^{f}	2.295(12)	U4–O15^{f}	2.299(12)
U1–O6	2.566(12)	U2–O3^{d}	2.483(12)	U3–O9	2.336(14)	U4–O6^{f}	2.477(13)
U1–O3^{b}	2.607(12)	U2–O6	2.509(13)	U3–O4^{d}	2.431(12)	O13═U5═O14	178.4(5)
O1═U1═O2	178.5(5)	O7═U2═O8	177.0(5)	O10═U4═O11	175.3(5)		
Mg1–O16^{g}	2.051(11)	Mg1–O11^{g}	2.061(12)	Na1–O2^{h}	2.412(15)	Na1–O7^{c}	2.501(13)
Mg1–O16	2.051(11)	Mg1–O17	2.120(12)	Na1–O10	2.439(15)	Na1–O8^{h}	2.634(14)
Mg1–O11	2.061(12)	Mg1–O17^{g}	2.120(12)	Na1–O14^{f}	2.450(15)	Na1–O13	2.931(16)

^{a} −*X*, 1 − *Y*, 2 − *Z*. ^{b} −*X*, −*Y*, 2 − *Z*. ^{c} 1 − *X*, 1 − *Y*, 2 − *Z*. ^{d} +*X*, 1 + *Y*, +*Z*. ^{e} 1 − *X*, 2 − *Y*, 1 − *Z*. ^{f} 1 − *X*, 1 − *Y*, 1 − *Z*. ^{g} −*X*, 2 − *Y*, 1 − *Z*. ^{h} 1 + *X*, +*Y*, +*Z*.

other synthetic UOH systems especially with the presence of β-U_3O_8 type layers.[16]

The bond valence sum (BVS) calculations (Table S1, ESI†) with the parameters from the literature[60,61] confirmed that all six U centres are present as U^{6+} [U1 (5.59), U2 (6.09), U3 (5.84), U4 (5.75), U5 (6.07) and U6 (6.05)] and two Mg centres as Mg^{2+} [Mg1 (2.29) and Mg2 (2.31)]. The asymmetric unit contains 2Mg, 6U and 30O (Table S1, ESI†), with the majority being O, two OH (O19 and O20) and eight H_2O (O23–O30). As such, the formula for **U-Mg1** was determined to be $Mg_2(H_3O)_2(H_2O)_6[(UO_2)_3O_4(OH)]_2$.

U-Mg2p crystallises in the triclinic $P\bar{1}$ space group. The layered crystal structure (Fig. 3a) is constructed by a unique type of uranium oxide hydroxide layer containing both α-U_3O_8 and β-U_3O_8 features (Fig. 3b) with alternating layers of 6-fold coordinated Mg^{2+} ions and both 6- and 8-fold coordinated Na^{+} ions (Fig. 3a and c). The structure contains six unique U centres, U1 in 6-fold coordination with a tetragonal bipyramid and U2–U6 in 7-fold coordination with pentagonal bipyramids. All six uranyl moieties exhibit the normal uranyl form with near-linear U═O bonds ranging from 1.808(9) to 1.851(9) Å and O═U═O angles from 175.2(5)° to 1778.1(4)°. The U–O bonds in the equatorial planes range from 2.192(9) to 2.743 (11) Å. The longer than normal U–O bonds of 2.743(11) Å for U2–O9 and 2.692(9) Å for U4–O14 are likely due to the deviations of O9 and O14 from the UOH layer. The Mg^{2+} ion is

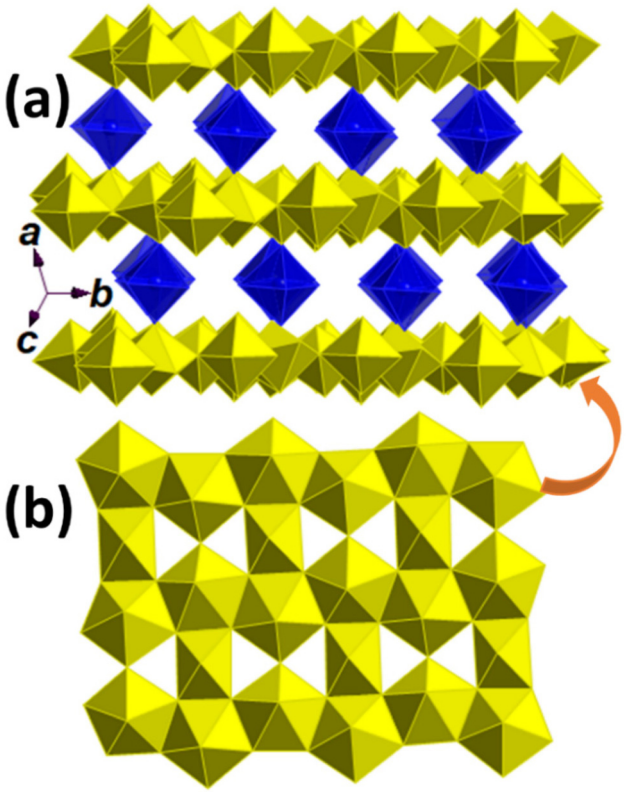

Fig. 2 Crystal structure of **U-Mg1**: a polyhedral view of the layered crystal structure with 6-fold coordinated Mg^{2+} interlayer cations (a), and the β-U_3O_8 type uranyl oxide hydroxide layer (b); U in yellow and Mg in blue.

6-fold coordinated in an octahedral environment with Mg–O bonds ranging from 2.029(10) to 2.127(10) Å. While Na1 is 6-fold coordinated in an octahedral geometry with Na–O bonds ranging from 2.235(11) to 2.672(11) Å, Na2 is 8-fold coordinated in a distorted cubic geometry with Na–O bonds ranging from 2.391(11) to 2.746(12) Å. All Mg–O and Na–O bond lengths are normal.

The distances between uranium oxide hydroxide layers are ~4.02 Å with interlayer Mg^{2+} cations and ~2.65 Å with interlayer Na^+ cations. The longer interlayer distance between the layers which sandwich Mg^{2+} cations is due to the corner-connections to the two most separated apices of the Mg octahedra. The BVS values (Table S2, ESI†) confirmed that all six U centres are present as U^{6+} [U1 (5.75), U2 (5.97), U3 (5.85), U4 (5.92), U5 and U6 (5.97)], the Mg centre as Mg^{2+} (2.21) and two Na centres as Na^+ [Na1 (1.02) and Na2 (1.14)], with the majority being O, four OH (O8, O9, O14 and O17) and four H_2O (O23–O26). The formula for **U-Mg2p** was then determined to be $Na_2Mg(H_2O)_4[(UO_2)_3O_3(OH)_2]_2$.

U-Mg2n crystallises in the triclinic $P\bar{1}$ space group. The layered structure (Fig. 4a) is constructed by a unique uranium oxide hydroxide layer (Fig. 4b) that is composed of two types of chains containing double U1 and U2, and double U3 and U4 (Fig. 3c) with mixed 6-fold coordinated Mg^{2+} and 7-fold coordinated Na^+ interlayer cations (Fig. 4d). There are four unique U centres, U1–U3 in pentagonal bipyramids and U4 in a tetragonal bipyramid, one 6-fold coordinated Mg and one 7-fold coordinated Na centre. All four uranyl centres are normal with U=O bond lengths from 1.792(13) to 1.861(13) Å and O=U=O angles from 175.3(5)° to 178.5(5)°. The equatorial U–O bond lengths range from 2.168(13) to 2.566(12) Å, which are typical U–O distances as previously reported.[16] While all six Mg–O bond lengths are in the normal range of 2.051(11) Å to 2.120(12) Å, the Na–O bond lengths are normal ranging from 2.412(15) Å to 2.931(16) Å.

The BVS values (Table S3, ESI†) confirmed that all four U centres are present as U^{6+} [U1 (5.90), U2 (6.00), U3 (5.86) and

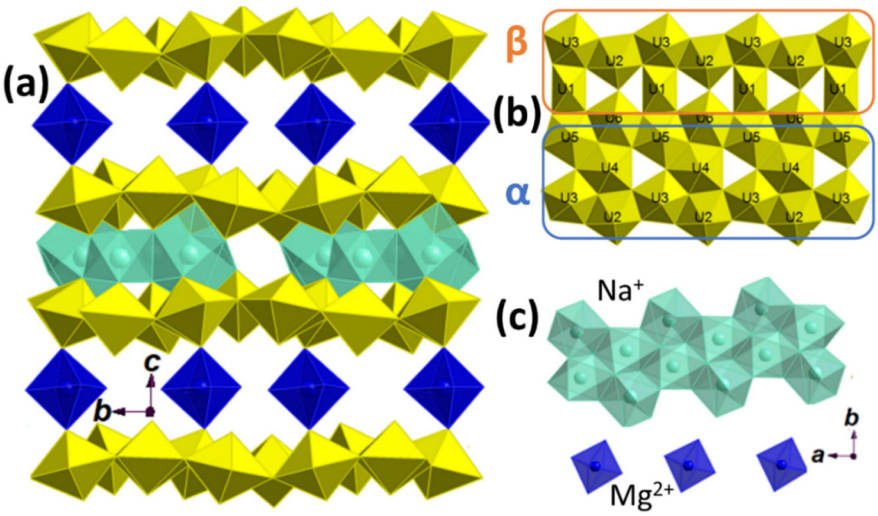

Fig. 3 Crystal structure of **U-Mg2p**: a polyhedral layered crystal structure along the *a*-axis (a), the uranium oxide hydroxide layer with a combination of α-U_3O_8 and β-U_3O_8 features (b), and alternating layers of isolated 6-fold coordinated Mg^{2+} cations, and both 6-fold and 8-fold coordinated Na^+ cations (c); U in yellow, Mg in blue and Na in light green.

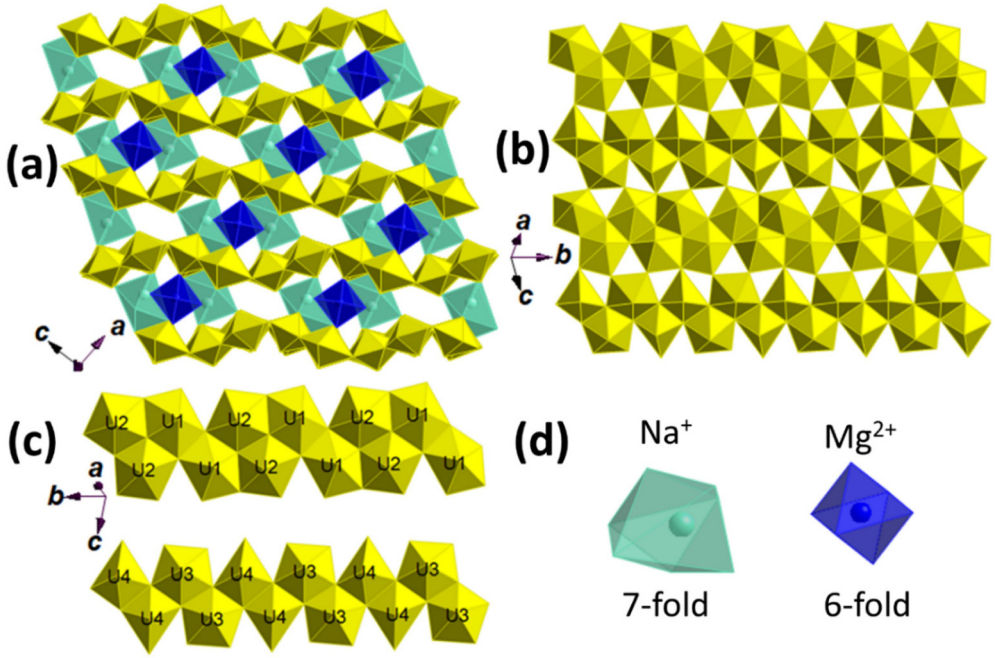

Fig. 4 Crystal structure of **U-Mg2n**: a polyhedral view of the layered structure along the *b*-axis (a), the uranium oxide hydroxide layer (b) constructed by corner-sharing two types of ribbons repeatedly which are built with edge-sharing double U1 and U2 and edge-sharing double U3 and U4 polyhedra (c), and 7-fold coordinated Na^+ ions and 6-fold coordinated Mg^{2+} ions as interlayer species (d); U in yellow, Mg in blue and Na in light green.

U4 (5.62)], Mg as Mg^{2+} (2.13) and Na as Na^+ (0.85), with three O (O5, O12 and O15) and four OH (O3, O4, O6 and O9) in the asymmetric unit. Consequently, the formula for **U-Mg2n** was determined to be $Na_2Mg(H_2O)_4[(UO_2)_4O_3(OH)_4]_2$.

3.2.1 UOH layers and layer topologies. Apart from common α-U_3O_8 and β-U_3O_8 types of UOH layers,[15,16] other unique types of layers and layer topologies have also been observed in some UOH minerals.[15,23] In this work, three types of UOH layers have been achieved: β-U_3O_8 for **U-Mg1**, a combination of α-U_3O_8 and β-U_3O_8 for **U-Mg2p**, and a corrugating one for **U-Mg2n** (Fig. 5). The β-U_3O_8 layer (Fig. 5a and d) is commonly found and overwhelmingly favoured in synthetic UOHFs,[39–43] largely due to its flexibility to accommodate possible lower valence states of uranium within the structures.[23–25] As such, it is also favoured in pseudo-UOHF materials such as synthetic UOH materials with Tb^{3+} or Ni^{2+} ions which act as interlayer pillars.[31,62] By increasing the solution pH from 6.5 to 8.0, two unique types of UOH layers were stabilised. **U-Mg2p** adopts a unique UOH layer (Fig. 5b and e) with combined α-U_3O_8 and β-U_3O_8 features, a new UOH layer identified for the first time to our knowledge. The corrugating UOH layer for **U-Mg2n** (Fig. 5c and f) was previously identified in a synthetic UOH compound, $Ca(UO_2)_4O_3(OH)_4(H_2O)_2$.[26] It should be noted that the U–O interatomic distance of 2.797 Å was used as the cut-off to define the uranium polyhedra, based on the longest U–O bond length identified for uranyl ions bonded to oxygen atoms in the ICSD.[63] The co-existence of the two types of UOH layers in one pot under the same synthesis conditions highlights the complex chemistry behind the formation of various UOH layers which dominate the stabilisation of UOH materials with secondary metal ions.

3.2.2 Secondary metal ions. Alkali metal ions such as Na^+ and K^+ with similar ionic radii to those of alkaline earth ions (Mg^{2+}, Ca^{2+} and Sr^{2+}) and metal ions (Pb^{2+} and Ln^{3+}) readily found in the surrounding of SNF under geological disposal could provide additional stability and flexibility to a variety of UOH structures by offering an additional charge compensation. Among all known UOH minerals, only richetite (Table 6) contains substantial amounts of Mg. Although several UOH minerals contain both alkali and alkaline earth metal ions (Table 6), few UOH minerals contain both Mg^{2+} and Na^+ ions. As such, this work fills the knowledge gaps not only for UOH materials with Mg^{2+} ions, but also for UOH materials containing both Mg^{2+} and Na^+ ions.

Unlike the Mg^{2+} ion which has a preferred octahedral coordination environment with the typical average Mg–O bond length of around 2.03 Å, the Na^+ ion is rather flexible adopting 6-/8-fold coordination geometries with longer Na–O bond lengths ranging from 2.38 to 2.93 Å. In addition, the single charge of the Na^+ ion makes it ready to be incorporated in various UOH structures for variable charge compensations.

3.3. TEM characterisation

In general, UOH materials are not stable in the ultra-high vacuum of the TEM and beam damage is likely to occur, making the TEM analysis rather difficult. However, the strategy of minimising working time and working on multiple grains seems to be a good practice often leading to success.

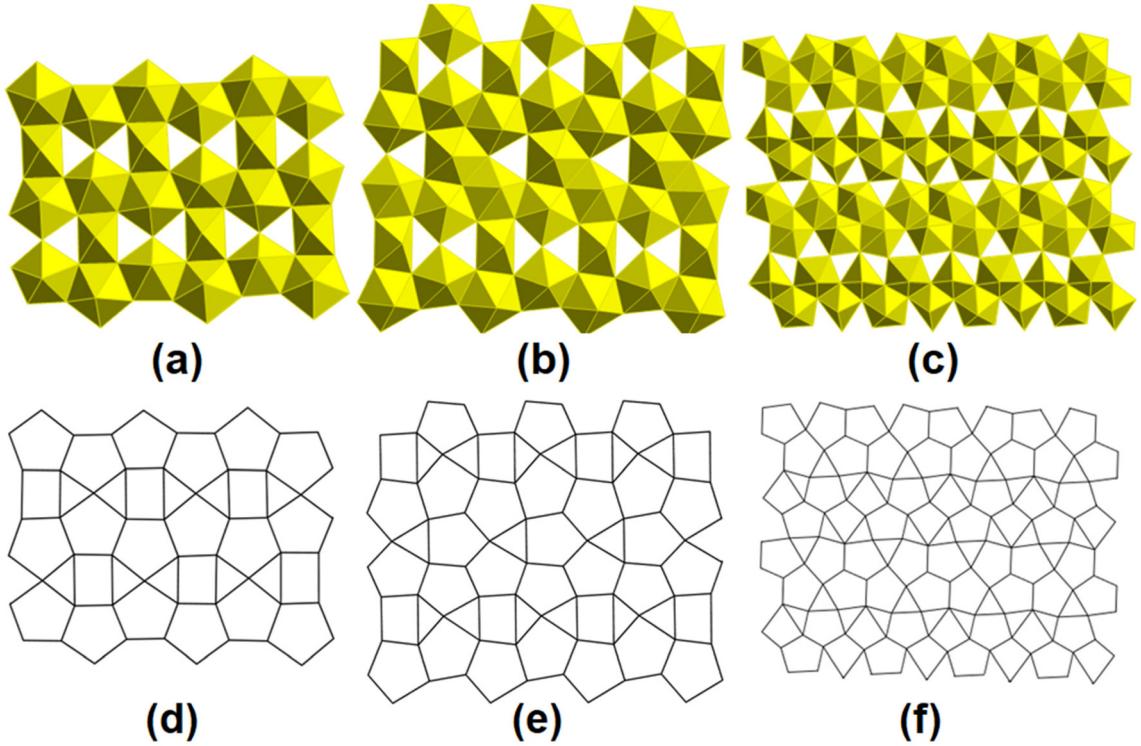

Fig. 5 The three types of uranium oxide hydroxide layers and their corresponding anionic topologies identified in this work: β-U_3O_8 in **U-Mg1** (a and d), a combination of α-U_3O_8 and β-U_3O_8 in **U-Mg2p** (b and e), and an undulating one in **U-Mg2n** (c and f).

Table 6 Uranium oxide hydrate minerals with both alkali and alkaline earth metal ions

Mineral	Chemical formula	Space group	Cell parameters	Ref.
Agrinierite	$K_2(Ca_{0.65}Sr_{0.35})[(UO_2)_3O_3(OH)_2]_2(H_2O)_5$	Orthorhombic, *F*2*mm*	a = 14.094(2), b = 14.127(2), c = 24.106(4) Å (Z = 16), V = 4799.6(1) Å^3	19
Calciouranoite	(Ca, Ba, Pb, K_2, Na_2)$[(UO_2)(O,OH)](H_2O)_5$	—	—	50
Metacalciouranoite	(Ca, Ba, Pb, K_2, Na_2)$[(UO_2)(O,OH)](H_2O)_2$	—	—	50
Clarkeite	(Na, Ca)$[(UO_2)(O,OH)](H_2O)_{0-1}$	Hexagonal, $R\bar{3}w$	a = 3.954(4), c = 17.73(1) Å (Z = 3)	51
Rameauite	$K_2Ca[(UO_2)_6O_6(OH)_4](H_2O)_6$	Monoclinic, *C*2/*c*	a = 13.97, b = 14.26, c = 14.22 Å, β = 121°	20
Richetite	$(Fe,Mg)_xPb_{8.57}[(UO_2)_{18}O_{18}(OH)_{12}]_2(H_2O)_{41}$	Triclinic, *P*1	a = 20.9391(3), b = 12.1000(2), c = 16.3450(3) Å, α = 103.87(1), β = 115.37(1), γ = 90.27(1)°, V = 3605.2 Å^3	47

Compounds **U-Mg1** and **U-Mg2n** were further examined by TEM. For **U-Mg1**, a TEM bright field image showed the **U-Mg1** grains (Fig. S4a, ESI†). The selected area electron diffraction (SAED) pattern in a single zone axis was not obtained even using the smallest selected aperture; instead, diffraction rings were obtained (Fig. S4b, ESI†). Additionally, several bright spots on the rings indicated that the grain size of **U-Mg1** is very fine as the smallest selected aperture contains several grains for diffraction. However, the d-spacing distances measured from the TEM diffraction rings agree with the SC-XRD result for the **U-Mg1** crystal structure in the $P2_1/c$ space group. A high-resolution transmission electron microscopy (HRTEM) image showed lattice fringes in nano-domains (Fig. S4c, ESI†).

For **U-Mg2n**, a TEM bright field image (Fig. 6a) showed the crushed grains. TEM-EDS analysis confirmed the presence of U, Mg, Na and O. The SAED pattern from a grain in the [3 1 1] zone axis was indexed to the triclinic $P\bar{1}$ space group (Fig. 6b), in agreement with the SC-XRD pattern. A HRTEM image in the [−1 1 1] zone axis showed lattice fringes with a fast Fourier transform (FFT) image in the inset (Fig. 6c). The d(2 2 0) and d(2 0 2) spacing values of 0.324 nm and 0.312 nm measured from the image (Fig. 6c) are consistent with the crystal data from SC-XRD.

3.4. Electronic structures

Based on BVS calculations, all three compounds are U^{6+} dominant and the characteristic feature in the DRS spectra (Fig. 7) is the broad and unresolved absorptions in the UV region (300 nm–500 nm) with two broad maxima at ~350 nm and ~450 nm, corresponding to the typical charge transfer bands for the U^{6+} containing materials.[64–69]

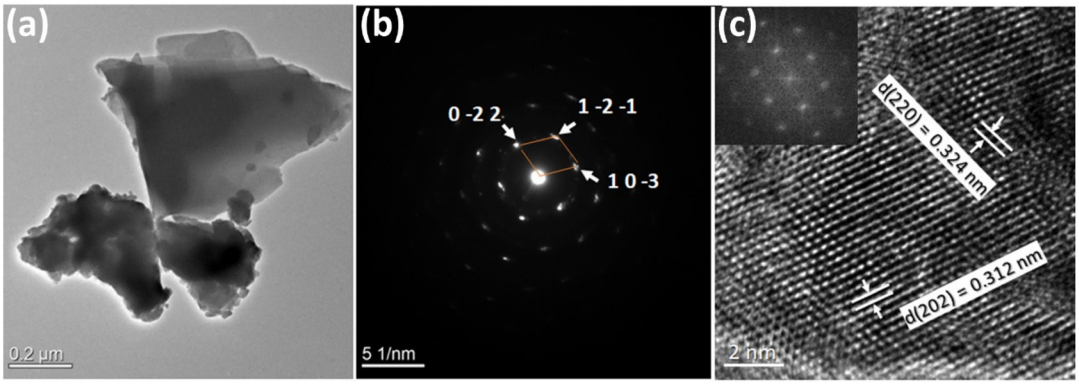

Fig. 6 TEM of **U-Mg2n**: a TEM bright field image of grains (a), a SAED pattern from a grain in the [3 1 1] zone axis indexed to the crystal structure in the $P\bar{1}$ space group (b), and a HRTEM image in the [−111] zone axis with a fast Fourier transform (FFT) image in the inset (c).

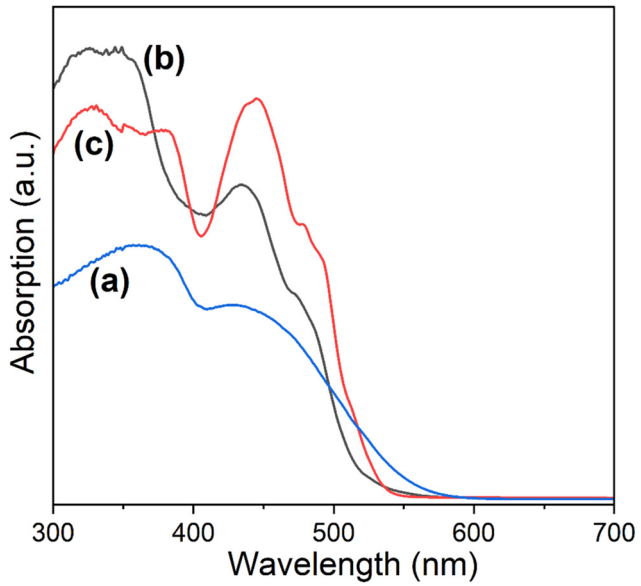

Fig. 7 DRS spectra of **U-Mg1** (a), **U-Mg2p** (b) and **U-Mg2n** (c) in the UV-vis region.

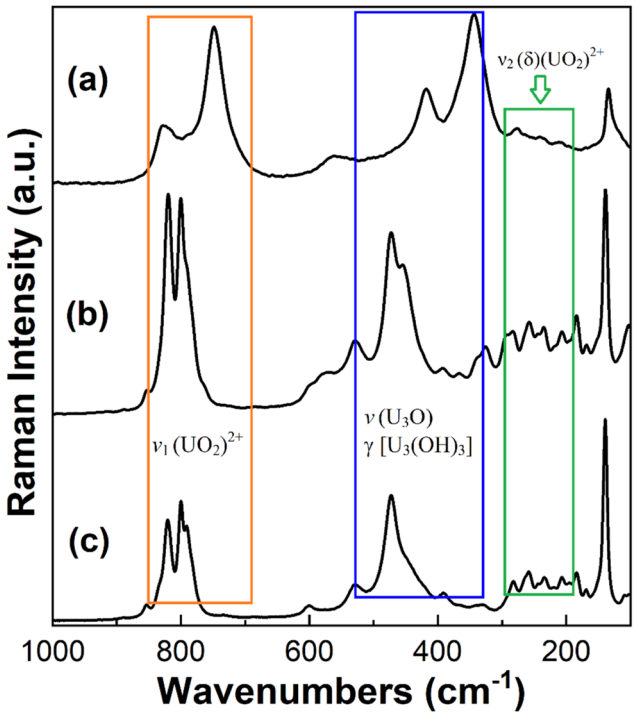

Fig. 8 The Raman spectra of **U-Mg1** (a), **U-Mg2p** (b) and **U-Mg2n** (c).

3.5. Vibrational modes

Micro-Raman spectroscopy has been used to study the vibrational modes of compounds **U-Mg1**, **U-Mg2p** and **U-Mg2n**. Raman spectra for **U-Mg1**, **U-Mg2p** and **U-Mg2n** (Fig. 8) have revealed multiple bands at 850–700 cm^{-1},[70–72] corresponding to a variety of calculated U=O bond lengths for the uranyl centres between 1.762 Å and 1.854 Å,[73] broadly consistent with the U=O bond lengths (1.792 Å–1.861 Å) determined from the SC-XRD analysis. The bands at 520–310 cm^{-1} have been assigned predominantly to $\nu(U_3O)$ bridge elongations and $\gamma[U_3(OH)_3]$ bending vibrations,[70–72] and possibly $\nu(U–O_{ligand})$ vibrations. Multiple weak bands at 295–200 cm^{-1} are due to $\nu_2(UO_2)^{2+}$ bending vibrations while lattice vibrations can be seen below 150 cm^{-1}.[70–72]

3.6. Implications and perspectives

It is essential to understand the alteration chemistry of uranium oxides in the presence of transition metal ions given their abundance in the environment. With only a few UOH materials containing transition metal ions being reported,[31–34] there is an obvious need for further work. Many bivalent 3d/4d-transition metal ions (M^{2+} = Mn, Co, Ni, Cu, Zn, Cd) have ionic radii ranging from 0.69 to 0.95 Å with the corresponding $r(M^{2+})/r(O^{2-})$ ratios in the range 0.73–0.41, characteristic of the octahedral coordination geometry for M^{2+} ions.[49] The Mg^{2+} ion is of particular interest as its ionic radius also meets the conditions for octahedral coordination [$r(Mg^{2+})$ = 0.72 Å, $r(Mg^{2+})/r(O^{2-})$ = 0.53]. As such, all synthetic UOH-Mg phases will be very useful in predicting the potential formation of UOH phases with bivalent transition metal ions.

Many UOH minerals containing dual or multiple cations have been well documented due to their relative abundance in

the geological environment. Despite this, only a few synthetic UOH materials with dual cations have been reported, clearly highlighting the need to further explore UOHs with dual cations. The importance of exploring dual-cation systems has been demonstrated in this work by maintaining the same Na : Mg ratio (2 : 1) within the two different structures in a one pot synthesis. As such, these dual-cation systems deserve further study.

Uranyl hydrolysis is heavily pH dependent. Hydrolysed uranyl species such as $[UO_2(OH)]^+$, $[(UO_2)(OH)_2]$, $[(UO_2)_2(OH)_2]^{2+}$ and $[(UO_2)_3(OH)_5]^+$ increase when the solution pH is above 5.[33] Most of the UOH phases were synthesised hydrothermally with solution pH values from 3 to 6. However, UOH phase formation in slightly alkaline solutions has been less investigated. This was briefly addressed in this work by furthering uranyl hydrolysis at solution pH values from 6.5 to 8.0. The success in synthesising the three novel UOHs with Mg^{2+} ions highlights the delicate balance of reaction conditions which leads to the formation of preferred structure types. Future synthesis work targeting higher solution pH values (from 8 to 10) close to the pH range for underground water is essential towards elucidating the conditions that drive the selective formation of new UOH phases.

4. Conclusions

Three novel UOH materials with Mg^{2+} or Mg^{2+} and Na^+ ions have been successfully synthesised hydrothermally, with the solution pH adjusted by adding a dilute NaOH solution. Although they are all layered structures with interlayer secondary cations, they differ substantially in the uranium oxide hydroxide layers and the arrangements of interlayer cations. While **U-Mg1** crystallises in the $P2_1/c$ space group with a U : Mg ratio of 3 : 1, both **U-Mg2p** and **U-Mg2n** crystallise in the $P\bar{1}$ space group with U : Mg : Na ratios of 6 : 1 : 2 and 8 : 1 : 2, respectively. The structures differ in that **U-Mg1** has β-U_3O_8-type uranyl oxide hydroxide layers with Mg^{2+} interlayer cations while **U-Mg2p** has unique layers containing both α-U_3O_8 and β-U_3O_8 features, and **U-Mg2n** has corrugated layers but with different ways of incorporating mixed Mg^{2+} and Na^+ interlayer cations.

The structure diversity in the U–Mg system has been achieved in a narrow solution pH range from 6.5 to 8.0, highlighting the complex uranium chemistry which drives the formation and stabilisation of UOH phases at near neutral solution pH values *via* the subtle evolution of uranium oxide hydroxide layers and the incorporation of single-/dual-secondary cations. While the Mg^{2+} ion adopts 6-fold coordination in an octahedral geometry similar to some 3d transition metal ions (such as Co^{2+} and Ni^{2+}), the Na^+ ion adopts more flexible coordination environments with coordination numbers ranging from 6 to 8. Therefore, this work not only fills the knowledge gaps in synthetic UOH phases with Mg^{2+} ions, but also sheds light on the possible UOH structures with some 3d transition metal ions (a similar coordination environment to the Mg^{2+} ion). Although the structural flexibility induced by the addition of Na^+ ions has been briefly discussed, further work on dual-cation systems is still necessary to better rationalise the complex structural nature of these UOH phases. In addition, further experiments such as X-ray absorption could resolve ambiguities in these complex structures, such as whether they have variable compositions.

Author contributions

Y. Zhang: conceptualization, data curation, formal analysis, project administration, resources, supervision, writing – original draft, and writing – review & editing; K. T. Lu: data curation, formal analysis, and writing – review & editing; T. Wei: data curation, formal analysis, and writing – review & editing; I. Karatchevtseva: data curation, formal analysis, and writing – review & editing; R. Zheng: supervision and writing – review & editing.

Conflicts of interest

The authors are not aware of any conflict of interest.

Acknowledgements

The synthesis and characterization of materials were carried out in the facilities under Nuclear Science and Technology (NST) at ANSTO. The crystallographic data for compounds **U-Mg1**, **U-Mg2p** and **U-Mg2n** were collected on the MX2 beamline at the Australian Synchrotron, a part of ANSTO, and the Australian Cancer Research Foundation (ACRF) detector was used.

References

1 V. Popa and O. Cocoş, *Cent. Eur. J. Geogr. Sustainable Dev.*, 2021, **3**, 17–25.
2 Y. Zhang, L. Kong, M. Ionescu and D. J. Gregg, *J. Eur. Ceram. Soc.*, 2022, **42**(5), 1852–1876.
3 R. J. Baker, *Coord. Chem. Rev.*, 2014, **266**, 123–136.
4 S. Spiridonov, A. Perevolotskii, T. Perevolotskaya, R. Aleksakhin and E. Spirin, *At. Energy*, 2017, **123**, 122–126.
5 A. Paulillo, J. M. Dodds, S. J. Palethorpe and P. Lettieri, *Sustainable Mater. Technol.*, 2021, **28**, e00278.
6 D. Mallants, K. Travis, N. Chapman, P. V. Brady and H. Griffiths, *Energies*, 2020, **13**(4), 833.
7 J. Plášil, *J. Geosci.*, 2014, **59**, 99–114.
8 J. Janeczek and R. C. Ewing, *J. Nucl. Mater.*, 1992, **190**, 128–132.
9 R. J. Finch, R. Haddal and G. T. Baldwin, Safeguards Implications for Deep Borehole Disposal of Spent Fuel, SAND2016-4591 report, 2016, Sandia National Laboratories, USA.

10 R. C. Ewing, *Nat. Mater.*, 2015, **14**, 252–257.
11 D. J. Wronkiewicz, J. K. Bates, S. F. Wolf and E. C. Buck, *J. Nucl. Mater.*, 1996, **238**, 78–95.
12 R. J. Finch and R. C. Ewing, *J. Nucl. Mater.*, 1992, **190**, 133–156.
13 J. Janeczek and R. Ewing, *J. Nucl. Mater.*, 1992, **190**, 157–173.
14 J. Plášil, *Eur. J. Mineral.*, 2017, **29**, 1–15.
15 P. C. Burns, Hydrated uranium oxides, in *Comprehensive Nuclear Materials*, ed. R. Konings and R. Stoller, Elsevier, 2nd edn, 2020.
16 Y. Zhang, K. T. Lu and R. Zheng, *Dalton Trans.*, 2022, **51**, 2158–2169.
17 T. A. Olds, J. Plášil, A. R. Kampf, T. Spano, P. Haynes, S. M. Carlson, P. C. Burns, A. Simonetti and O. P. Mills, *Am. Mineral.*, 2018, **103**, 143–150.
18 P. C. Burns, *Can. Mineral.*, 1998, **36**, 1061–1067.
19 C. L. Cahill and P. C. Burns, *Am. Mineral.*, 2000, **85**, 1294–1297.
20 J. Plášil, R. Škoda, J. Čejka, V. Bourgoin and J.-C. Boulliard, *Eur. J. Mineral.*, 2016, **28**, 959–967.
21 K. A. Hughes, P. C. Burns and U. Kolitsch, *Can. Mineral.*, 2003, **41**, 677–685.
22 J. Plášil, *Eur. J. Mineral.*, 2018, **30**, 237–251.
23 M. L. Miller, R. J. Finch, P. C. Burns and R. C. Ewing, *J. Mater. Res.*, 1996, **11**(12), 3048–3056.
24 P. C. Burns and F. C. Hill, *Can. Mineral.*, 2000, **38**, 163–173.
25 F. C. Hill and P. C. Burns, *Can. Mineral.*, 1999, **37**, 1283–1288.
26 R. E. Glatz, Y. Li, K.-A. Hughes, C. L. Cahill and P. C. Burns, *Can. Mineral.*, 2002, **40**, 217–224.
27 P. C. Burns and F. C. Hill, *Can. Mineral.*, 2000, **38**, 175–181.
28 K. T. Lu, Y. Zhang, T. Wei, T. A. Ablott, T. H. Nguyen and R. Zheng, *New J. Chem.*, 2022, **46**, 1371–1380.
29 K. T. Lu, Y. Zhang, T. Wei, T. A. Ablott, J. Plasil, I. Karatchevtseva and R. Zheng, *New J. Chem.*, 2023, **47**, 13286–13296.
30 Y. Li and P. C. Burns, *Can. Mineral.*, 2000, **38**, 1433–1441.
31 M. Rivenet, N. Vigier, P. Roussel and F. Abraham, *J. Solid State Chem.*, 2009, **182**, 905–912.
32 N. G. Chernorukov, O. V. Nipruk, K. A. Klinshova, O. N. Tumaeva and D. V. Sokolov, *New J. Chem.*, 2021, **45**, 9922–9935.
33 T. A. Ablott, K. T. Lu, T. Wei and Y. Zhang, *Dalton Trans.*, 2023, **52**, 6629–6640.
34 Y. Zhang, J. Čejka, G. R. Lumpkin, T. T. Tran, I. Aharonovich, I. Karatchevtseva, J. R. Price, N. Scales and K. Lu, *New J. Chem.*, 2016, **40**, 5357–5357.
35 Y. Zhang, R. Aughterson, I. Karatchevtseva, L. Kong, T. T. Tran, J. Čejka, I. Aharonovich and G. R. Lumpkin, *New J. Chem.*, 2018, **42**, 12386–12393.
36 Y. Zhang, R. D. Aughterson, Z. Zhang, T. Wei, K. Lu, J. Čejka and I. Karatchevtseva, *Inorg. Chem.*, 2019, **58**, 10812–10821.
37 G. L. Murphy, P. Kegler, M. Klinkenberg, A. Wilden, M. Henkes, D. Schneider and E. V. Alekseev, *Dalton Trans.*, 2021, **50**, 17257–17264.
38 K.-A. Kubatko and P. C. Burns, *Inorg. Chem.*, 2006, **45**, 10277–10281.
39 T. A. Ablott, K. T. Lu, R. D. Aughterson and Y. Zhang, *Dalton Trans.*, 2022, **51**, 15965–15973.
40 Y. Li, C. L. Cahill and P. C. Burns, *Chem. Mater.*, 2001, **13**, 4026–4031.
41 K. T. Lu, Y. Zhang, R. D. Aughterson and R. Zheng, *Dalton Trans.*, 2020, **49**, 15854–15863.
42 K. T. Lu, Y. Zhang, T. Wei, Z. Wang, D. T. Oldfield and R. Zheng, *Inorg. Chem.*, 2021, **60**, 13233–13241.
43 Y. Zhang, T. Wei, T. T. Tran, K. T. Lu, Z. Zhang, J. R. Price, I. Aharonovich and R. Zheng, *Inorg. Chem.*, 2020, **59**, 12166–12175.
44 Magnesium, National Minerals Information Center, USGS, **https://www.usgs.gov/centers/national-minerals-information-center/magnesium-statistics-and-information**.
45 H. Steinfink and F. J. Sans, *Am. Mineral.*, 1959, **44**, 679–682.
46 Search Minerals By Chemistry (mindat.org).
47 P. C. Burns, *Can. Mineral.*, 1998, **36**, 187–199.
48 R. Vochten, L. Van Haverbeke and R. Sobry, *J. Mater. Chem.*, 1991, **1**(4), 637–642.
49 N. G. Chernorukov, O. V. Nipruk, G. N. Chernorukov and O. S. Sedelkina, *Radiochemistry*, 2015, **57**(4), 378–380.
50 L. N. Belova, B. I. Ryzhov, O. V. Fedorov and G. V. Lyubomilova, *Izv. Akad. Nauk SSSR, Ser. Geol.*, 1985, **2**, 65–72.
51 R. J. Finch and R. C. Ewing, *Am. Mineral.*, 1997, **82**, 607–619.
52 D. Aragão, J. Aishima, H. Cherukuvada, R. Clarken, M. Clift, N. P. Cowieson, D. J. Ericsson, C. L. Gee, S. Macedo, N. Mudie, S. Panjikar, J. R. Price, A. Riboldi-Tunnicliffe, R. Rostan, R. Williamson and T. T. Caradoc-Davies, *J. Synchrotron Radiat.*, 2018, **25**, 885–891.
53 W. Kabsch, *Acta Crystallogr., Sect. D: Biol. Crystallogr.*, 2010, **66**, 133–144.
54 G. M. Sheldrick, *SADABS, Empirical Absorption and Correction Software*, University of Göttingen, Göttingen, 1996.
55 G. M. Sheldrick, *Acta Crystallogr., Sect. A: Found. Adv.*, 2015, **71**, 3–8.
56 G. M. Sheldrick, *Acta Crystallogr., Sect. C: Struct. Chem.*, 2015, **71**, 3–8.
57 O. V. Dolomanov, L. J. Bourhis, R. J. Gildea, J. A. K. Howard and H. Puschmann, *J. Appl. Crystallogr.*, 2009, **42**, 339–341.
58 S. Wu, J. Ling, S. Wang, S. Skanthakumar, L. Soderholm, T. E. Albrecht-Schmitt, E. V. Alekseev, S. V. Krivovichev and W. Depmeier, *Ber. Dtsch. Chem. Ges.*, 2009, **27**, 4039–4042.
59 Z. Weng, S. Wang, J. Ling, J. M. Morrison and P. C. Burns, *Inorg. Chem.*, 2012, **51**, 7185–7191.
60 I. D. Brown, *Chem. Rev.*, 2009, **109**(12), 6858–6919.
61 P. C. Burns, P. C. Burns, R. C. Ewing and F. C. Hawthorne, *Can. Mineral.*, 1997, **35**, 1551–1570.
62 K. T. Lu, Y. Zhang, T. Wei, J. Čejka and R. Zheng, *Dalton Trans.*, 2020, **49**, 5832–5841.
63 O. C. Gagné, *Acta Crystallogr., Sect. B: Struct. Sci., Cryst. Eng. Mater.*, 2018, **74**, 49–62.
64 Y. Zhang, D. J. Fanna, N. D. Shepherd, I. Karatchevtseva, K. Lu, L. Kong and J. R. Price, *RSC Adv.*, 2016, **6**, 75045–75053.

65 N. D. Shepherd, Y. Zhang, I. Karatchevtseva, J. R. Price, L. Kong, N. Scales and G. R. Lumpkin, *Polyhedron*, 2016, **113**, 88–95.
66 E. R. Vance, Y. Zhang and Z. Zhang, *J. Nucl. Mater.*, 2010, **400**(1), 8–14.
67 Y. Zhang, T. Wei, Z. Zhang, L. Kong, P. Dayal and D. J. Gregg, *J. Am. Ceram. Soc.*, 2019, **102**(12), 7699–7709.
68 Y. Zhang, L. Kong, I. Karatchevtseva, R. D. Aughterson, D. J. Gregg and G. Triani, *J. Am. Ceram. Soc.*, 2017, **100**(9), 4341–4351.
69 Y. Zhang, L. Kong, R. D. Aughterson, I. Karatchevtseva and R. Zheng, *J. Am. Ceram. Soc.*, 2017, **100**(11), 5335–5346.
70 R. L. Frost, J. Čejka and M. L. Weier, *J. Raman Spectrosc.*, 2007, **38**(4), 460–466.
71 Y. Zhang, J. Čejka, I. Karatchevseva, M. Qin, L. Kong, K. Short, S. C. Middleburg and G. R. Lumpkin, *J. Nucl. Mater.*, 2014, **446**, 68–72.
72 Y. Zhang, I. Karatchevtseva, M. Qin, S. C. Middleburgh and G. R. Lumpkin, *J. Nucl. Mater.*, 2013, **437**, 149–153.
73 J. R. Bartlett and R. P. Cooney, *J. Mol. Struct.*, 1989, **193**, 295–300.